International Journal of Geo-Information

MDPI

Article

Intensity and Direction of Land-Use Conflicts Across China: Spatiotemporal Patterns and Associated Factors

Wenxu Wu [1,2], Peng Ti [1,*], Hong Chen [2], Yong Dong [2], Hongguo Jia [1] and Yining Zhang [3]

[1] Faculty of Geosciences and Engineering, Southwest Jiaotong University, Chengdu 611756, China; wuwenxu999@my.swjtu.edu.cn (W.W.)
[2] Faculty of Geomatics, Lanzhou Jiaotong University, Lanzhou 730070, China
[3] School of Architecture, Southwest Jiaotong University, Chengdu 611756, China
* Correspondence: pti@swjtu.edu.cn

Abstract

Understanding land-use conflicts requires identifying both the magnitude of suitability–use divergence and the functional relationship involved. Intensity-based assessments alone cannot distinguish functionally different mismatches. This study developed a direction-aware framework representing production, ecological, and living suitability and actual use within a common functional space. Vector divergence quantified conflict intensity, while the ordered pairing of dominant functions identified mismatch direction. The framework was applied across China at 1 km resolution for 2015, 2020, and 2024, with XGBoost–SHAP models examining associated environmental and socioeconomic conditions. The share of land experiencing moderate-to-severe conflicts declined from 57.67% to 47.33%, but functional mismatches persisted. Production-to-Ecology remained the dominant mismatch class, decreasing from 21.32% to 20.53% and predominating in Northwest and Southwest China, whereas East, Central, and Northeast China contained larger Living-to-Production components. Intensity and direction exhibited different explanatory profiles, with building density and aridity ranking consistently higher among the predictors of direction than of intensity. Joint assessment distinguishes the magnitude of suitability–use divergence from its functional configuration, revealing persistent mismatches obscured by aggregate intensity trends and supporting differentiated regional land-management assessment.

Keywords: land-use conflicts; production–ecological–living space; land suitability; functional mismatch direction; spatial analysis; explainable machine learning

Check for updates

Academic Editors: Wolfgang Kainz and Godwin Yeboah

Received: 27 September 2026
Revised: 19 November 2026
Accepted: 24 November 2026
Published: 27 November 2026

Copyright: © 2026 by the authors. Published by MDPI on behalf of the International Society for Photogrammetry and Remote Sensing. Licensee MDPI, Basel, Switzerland. This article is an open access article distributed under the terms and conditions of the Creative Commons Attribution (CC BY) license.

1. Introduction

Land-use decisions bear on food security, biodiversity conservation, and climate mitigation, yet nearly all land already provides benefits to society, so new demands compete with existing uses [1]. Land-use conflicts (LUCs) arise when competing demands for limited land cannot be simultaneously accommodated within the same territorial system [2]. Such conflicts are intensifying because these demands keep growing while the land base remains fixed: global food demand is projected to rise by 35–56% between 2010 and 2050 [3]. Urban land could likewise expand 1.8- to 5.9-fold during this century [4]. This growth is met largely by converting land that already serves other functions, through two pathways. First, cropland expands into ecological land: about half of the cropland added worldwide between 2003 and 2019 replaced natural vegetation and tree cover, mainly in Africa and South America [5]. In South America, soybean expansion has driven deforestation at the Amazon and Cerrado frontiers, which zero-deforestation supply-chain policies now seek to

halt [6]. More broadly, agricultural production overlaps with conservation priorities, while climate-driven changes in suitability may increase production pressure on land currently supporting other functions [7,8]. Second, cities expand onto cropland, which made up nearly half of the land urbanized worldwide between 1992 and 2016. The resulting loss of production equals the minimum annual food needs of at least 36 million people [9]. By 2030, urbanization is projected to consume cropland that is 1.77 times more productive than the global average, about 80% of it in Asia and Africa [10]. The effect also extends beyond the converted land, because displaced cropland is re-established elsewhere and the forest lost indirectly to urban expansion far exceeds the direct loss [11]. Comparable pressures occur in high-income regions, including urban peripheries in Europe [12] and expanding metropolitan areas in the western United States [13]. The European Union has responded with a target of no net land take by 2050 [14]. Together, these pathways show that LUCs threaten food security and ecological integrity simultaneously, and that a conflict between two land functions can propagate to a third. Effective management therefore depends on knowing how severe a conflict is, which functions it involves, and which function gives way.

In China, both pathways operate simultaneously on a land base that produces one-fourth of the world's food, a supply threatened by rapid farmland conversion [15]. In rapidly urbanizing regions, built-up expansion can intensify competition between settlement development, agricultural production, and ecological conservation [16,17]. Urban expansion onto cropland has already raised food-security risks [9,18]. In response, China has invested USD 378.5 billion in 16 sustainability programs covering 623.9 million hectares, mostly since 1998 [19]. As the largest developing country, it is also establishing a unified territorial spatial planning system, including permanent basic farmland and ecological protection red lines, to balance development and protection [20]. These pressures vary regionally: population and urban land concentrate southeast of the Hu Huanyong Line [21,22], and land-use change has had different ecological effects on its two sides [23]. Nationwide, these conflicts are manifested through competition and mismatch among production, ecological, and living functions. Understanding LUCs therefore requires attention to both their severity and the functional relationships underlying them.

Research on LUCs has developed along two complementary lines, one explaining why conflicts arise and the other mapping where they occur. Socially oriented studies use participatory mapping, stakeholder interviews, and dispute records to examine how preferences, competing interests, and institutional arrangements shape conflicts [24–26]. Fienitz and Siebert [27] showed that actors' opportunities to participate and their willingness to cooperate help explain whether conflicts in eastern Germany remain latent, become collaborative, or escalate. Bekele et al. [28] attributed conflicts in Ethiopian agro-pastoral areas to pasture scarcity and insecure tenure following large-scale land investments. Cegielska et al. [29] combined resident surveys with spatial analysis around Kraków and found agricultural land most exposed to suburbanization-related conflict. Spatially explicit studies translate land-use competition into mapped indicators, identifying conflict intensity, competing functions, and changes under observed or simulated conditions [17,30,31]. At the global scale, Hoang et al. [8], Zabel et al. [32], and Rehbein et al. [33] mapped where agriculture, cropland expansion, and renewable energy facilities overlap with conservation priorities. At regional scales, conflict is commonly derived from multi-criteria evaluation of land suitability. Cieślak [34] developed a multi-criteria index of conflict drivers for a rural municipality in Poland, and Luo et al. [35] combined suitability evaluation with interpretable machine learning for the Aral Sea Basin. In China, Dong et al. [36] and Lin et al. [37] extended suitability evaluation to resource scarcity and to production, ecological, and living functions. Jiang et al. [30] mapped the spatial and temporal patterns of conflict intensity and its drivers across China. Zong et al. [31] classified potential conflicts from

combinations of agricultural, construction, and ecological suitability, while Han et al. [38] distinguished structural and functional conflicts at the county level. Wang et al. [39] further combined ecological, agricultural, and urban functions with four intensity tiers to identify 12 conflict patterns nationwide. These approaches provide complementary information: intensity indices summarize the degree of conflict, while functional classifications identify the uses involved.

For suitability-based assessment, however, potential competition among suitable uses and mismatch between suitability and actual use represent different diagnostic questions. This distinction raises a further question: when assessed suitability and observed use differ, which function dominates each side of that relationship? Production-dominant suitability paired with ecology-dominant use and the reverse pairing involve the same functions but represent different mismatches. We therefore measure direction as the ordered pairing of suitability-dominant and actual-use-dominant functions, alongside the magnitude of their vector divergence. This multidimensional perspective is consistent with evidence that urban form–function compactness involves trade-offs between resource efficiency and ecological outcomes [40]. National assessments have documented pronounced regional differences in conflict intensity, associated factors, and potential conflict types [30,31,38,39]. Studies of urban–rural land transitions across China and construction-related fragmentation in mountain cities further show that land-use pressures take different forms across settings [16,41]. Yet neither these national patterns nor the global overlap maps [8,32,33] establish whether a decline in suitability–use divergence is accompanied by a change in the specific functional relationship involved. Applying the same grid-based measure of intensity and direction across China enables direct regional comparisons and reveals whether a national decline conceals persistent directional mismatches. We therefore ask whether changes in intensity coincide with closer functional alignment, and how this relationship differs among regions.

To address these questions, we develop and apply a direction-aware framework to 1 km grid cells across China in 2015, 2020, and 2024. In this study, land-use conflict refers to potential conflict, following the notion of land-use conflict potential [24,31]. It is a spatially diagnosed mismatch between assessed suitability and actual use within a grid cell. It does not represent a social dispute among stakeholders, nor does it judge whether the current land use is inappropriate. A mismatch may also result from deliberate planning, such as ecological restoration or conservation. We first assess production, ecological, and living suitability and represent actual land use in the same functional space. We then measure conflict intensity as vector divergence and classify mismatch direction from the ordered pairing of dominant functions. Direction thus distinguishes cells of equal intensity that involve different functional relationships and therefore call for different management assessments. The resulting maps allow us to compare temporal change and regional variation in both diagnostic dimensions. Finally, XGBoost and SHAP characterize the environmental and socioeconomic associations of intensity and individual directional classes [42]. This sequence examines whether an aggregate decline in intensity coexists with persistent functional mismatches.

2. Data and Methods

The analytical workflow consists of four modules (Figure 1). First, land-cover, biophysical, and socioeconomic layers were aligned to a common 1 km grid. Second, suitability and actual use in each grid cell were expressed as vectors of production, ecological, and living functions. Third, the divergence between the two vectors measured conflict intensity, and the ordered pairing of their dominant functions defined mismatch direction. Fourth, explanatory XGBoost models related intensity and direction to ten environmental and socioeconomic indicators, and SHAP interpreted these associations.

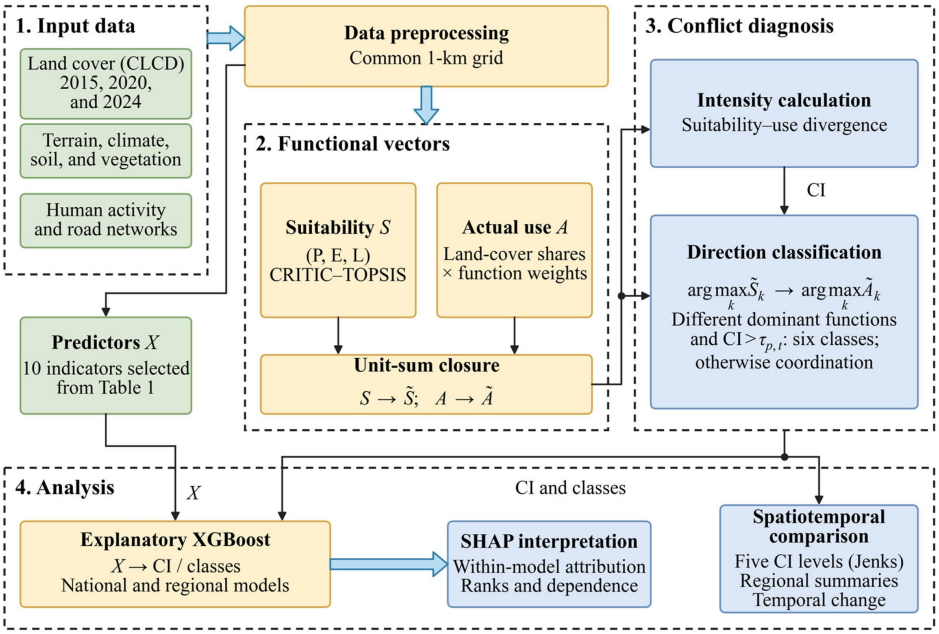


Figure 1. Technical roadmap for diagnosing the intensity and direction of land-use conflicts.

2.1. Study Area

China has undergone rapid urbanization and land-use transition over recent decades. Urban expansion, cropland protection, and ecological conservation have placed competing demands on the same land [16,30,38]. However, these demands do not fall evenly across the country, because China's population and land resources are distributed highly unevenly. The Hu Huanyong Line (Hu Line), which runs from Heihe in Heilongjiang Province to Tengchong in Yunnan Province, marks this contrast (Figure 2). Since it was proposed in 1935, the line has separated a densely populated southeast from a sparsely populated northwest, a pattern that has remained stable across national censuses [21,43]. In 2005, about 94% of China's urban land also lay southeast of the line [22]. In the southeast, limited suitable land faces intense competition among production, ecological, and living functions. The vast northwest, by contrast, is dominated by plateaus, deserts, and arid grasslands. Its suitability for agriculture and settlement is low, and most of the land serves ecological functions, including key national ecological barriers. Land-use change has accordingly produced different ecological effects on the two sides of the line [23]. These contrasts make China a suitable case for examining how the intensity and direction of land-use conflicts vary across regions and over time.

2.2. Data Sources and Preprocessing

We assembled land-cover, biophysical, and socioeconomic layers to construct the suitability and actual-use vectors and examine their associated conditions.

Land cover was obtained from the China Land Cover Dataset (CLCD), derived from Landsat imagery at 30 m resolution [44]. Its categories were mapped to production, ecological, and living functions. Building density (BLD) was derived from the CLCD impervious-surface class (class 8). It was calculated as the total impervious area within each 1 km grid cell (km^2 $cell^{-1}$), representing built-up cover.

CLCD provides annual land-cover maps of China at 30 m resolution under a consistent classification scheme, which supports comparison among the study years. Within each 1 km cell, the 30 m pixels resolve land-cover heterogeneity and yield class-specific area fractions. Its classes, including cropland, forest, grassland, water, and impervious surfaces, map directly onto the functional weights of the land-cover–function matrix.

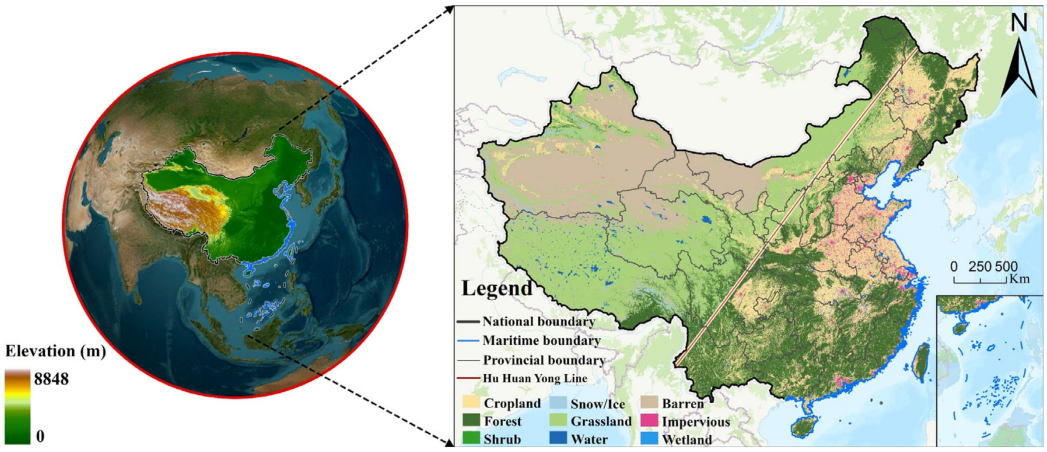


Figure 2. Study area and land-cover types in China in 2024.

Biophysical variables comprised terrain, climate, soil, and vegetation measures. Elevation and slope came from the 30 m GDEM V3 elevation model (http://www.gscloud.cn, accessed on 1 August 2025). Mean Annual Temperature (MAT) and Mean Annual Precipitation (MAP) were obtained from WorldClim at 1 km resolution [45]. The Aridity Index (AI) came from the Global Aridity Index Database V3 (CGIAR-CSI) [46]. Growing Degree Days (GDD) were calculated from MODIS/Terra 8-day Land Surface Temperature products on Google Earth Engine (GEE). Soil pH and Soil Organic Carbon (SOC) came from SoilGrids 2.0 at 250 m resolution [47]. The Normalized Difference Vegetation Index (NDVI) and Net Primary Productivity (NPP) were derived from MODIS products at 500 m native resolution and processed on GEE.

Nighttime Light (NTL) data represented socioeconomic activity. We used the cross-calibrated DMSP-OLS and SNPP-VIIRS series for China [48], extended to 2024 by its providers. Together, BLD and NTL represented the physical extent of development and socioeconomic activity, respectively [49]. OpenStreetMap (OSM) road networks supplied the hierarchy, density, and proximity measures used to calculate accessibility. The road networks were taken from historical OSM extracts provided by Geofabrik (https://download.geofabrik.de, accessed on 1 August 2025). Extracts dated 1 January 2016 and 1 January 2021 represent 2015 and 2020, and a 2024 extract represents 2024.

A 1 km × 1 km grid was used as the common analytical unit. Most indicator layers were available at 1 km resolution for analysis; layers with different resolutions were resampled and spatially aligned to the reference grid. Bilinear interpolation was used for continuous variables, whereas nearest-neighbor resampling was used where categorical layers required spatial alignment. For the 30 m CLCD data, land-cover composition was calculated by counting the pixels of each class within each 1 km grid cell and deriving their proportions. These proportions were combined with the land-cover–function matrix to construct the actual-use vectors, retaining information on the mixture of land-cover classes within each cell. For suitability assessment, continuous indicators were summarized as grid-level mean values using zonal statistics. Land-cover, BLD, and NTL inputs corresponded to 2015, 2020, and 2024, whereas elevation and slope were treated as static terrain variables.

2.3. Production–Ecological–Living Suitability Assessment

2.3.1. Multi-Indicator Evaluation

Suitability was evaluated for production, ecological, and living functions in each 1 km cell using multi-criteria evaluation (MCE). The indicators covered natural conditions, resource endowment, socioeconomic development, and infrastructure (Table 1). Production suitability denotes the capacity of a cell to support agricultural production, the production

function examined in national and global analyses of land-use conflict [8,31]. Industrial and commercial production enters as the secondary production weight of impervious surfaces (Table 2). Ecological suitability denotes the capacity of a cell to sustain ecosystem functions. It combines vegetation cover and productivity, water availability, terrain heterogeneity, low human disturbance, and the ecological weight of current land cover (Table 1). It therefore measures potential to sustain ecosystem functions. We standardized the indicators so that higher values consistently indicated greater suitability. Benefit indicators retained their normalized values; cost indicators were transformed using reciprocal or min–max normalization. Raw indicators were computed on a common basis nationwide. Normalization, CRITIC weighting, and TOPSIS were then performed separately for each province and year. Within each province-year, indicators were clipped at their 2nd and 98th percentiles before min–max scaling, which limits the influence of extreme values. Province-level evaluation adapts indicator ranges to the strong regional gradients across China and matches the province-year design of the diagnosis.

Table 1. Indicator system for evaluating the suitability of production, ecological, and living spaces.

Functional Category	Indicator	Unit	Direction	Description
Production space (PS)	Soil pH (PH)	–	+	Soil acidity–alkalinity condition, reflecting suitability for crop growth
	Soil organic carbon (SOC)	g/kg	+	Soil fertility and productivity potential
	Growing degree days (GDD)	°C·day	+	Thermal resources for agricultural production
	Precipitation (PRCP)	mm	+	Water availability for agricultural activities
	Slope (SLOPE)	°	–	Terrain constraints, steeper slopes reduce production suitability
	Elevation (DEM)	m	–	High altitudes restrict agricultural production
	Aridity index (AI)	–	+	Reflects climatic aridity; higher values indicate better suitability in semi-arid regions
	Accessibility (ACC)	–	+	Proximity to transportation networks, facilitating production activities
	Land use type (LANDUSE)	–	+	Production weight of the current land-cover classes in the land-cover–function matrix
Ecological space (ES)	Normalized Difference Vegetation Index (NDVI)	–	+	Vegetation cover and ecosystem stability
	Net primary productivity (NPP)	$gC/m^2 \cdot yr$	+	Ecosystem productivity and carbon sequestration capacity
	Precipitation (PRCP)	mm	+	Water availability for ecosystem maintenance
	Slope (SLOPE)	°	+	Topographic heterogeneity enhancing habitat diversity
	Elevation (DEM)	m	+	Altitudinal gradient supporting ecological heterogeneity
	Night-time light intensity (NTL)	$nW \cdot cm^{-2} \cdot sr^{-1}$	–	Human disturbance, higher values reduce ecological suitability
	Building density (BLD)	$km^2\ cell^{-1}$	–	Impervious-cover proxy of human pressure; negative for ecological suitability
	Land use type (LANDUSE)	–	+	Ecological weight of the current land-cover classes in the land-cover–function matrix
Living space (LS)	Night-time light intensity (NTL)	$nW \cdot cm^{-2} \cdot sr^{-1}$	+	Proxy for human activity and urbanization level
	Accessibility (ACC)	–	+	Transportation convenience for residential and service functions
	Building density (BLD)	$km^2\ cell^{-1}$	+	Impervious-cover proxy derived from CLCD; positive for living suitability
	Land use type (LANDUSE)	–	+	Living weight of the current land-cover classes in the land-cover–function matrix

Table 2. Land-cover–function matrix: weights of CLCD land-cover classes for production, ecological, and living functions.

Land-Cover Class	Production	Ecological	Living	Description
Cropland	0.9	0.1	0.0	Production-dominant; minor ecological function as an agroecosystem
Forest	0.2	0.8	0.0	Ecological-dominant; secondary production from timber and forest products
Shrub	0.2	0.7	0.1	Ecological-dominant; secondary production from fuelwood and grazing; minor living use
Grassland	0.3	0.6	0.1	Ecological-dominant; secondary production from grazing; minor living use in pastoral areas
Water	0.0	0.9	0.1	Ecological-dominant; minor living function through water supply and recreation
Snow/Ice	0.0	1.0	0.0	Ecological function only
Barren	0.1	0.9	0.0	Ecological-dominant; minor production from extensive grazing
Impervious surface	0.2	0.1	0.7	Living-dominant; secondary production from industrial and commercial land; minor ecological function
Wetland	0.1	0.8	0.1	Ecological-dominant; minor production (fisheries, reeds) and living (water supply, recreation) functions

CRITIC weights represented indicator variability and intercorrelation [50]. TOPSIS combined the weighted indicators using their relative distances from positive and negative ideal solutions [50,51]. The resulting production, ecological, and living suitability scores ranged from 0 to 1, with higher scores indicating greater suitability.

The indicator definitions, effect directions, and CRITIC–TOPSIS procedure were the same in all three study years, while the CRITIC weights were estimated from the data of each province and year. Because ranges are set within each province and year, temporal changes in suitability describe shifts in relative position within provinces.

2.3.2. Actual-Use Functional Composition

Actual-use functions were derived from the CLCD composition of each 1 km cell using a land-cover–function matrix (Table 2). Such matrices score the functions supplied by each land-cover class and are a standard way to translate land-cover maps into function maps [52,53]. In China, the classification of production, ecological, and living spaces follows the same logic and links each land-use type to the space it mainly serves [54–56]. It is commonly termed production–living–ecological (PLE) space. We built the matrix from this classification in two steps. First, each class was assigned the dominant function used consistently in national, regional, and global PLE studies [37,55,57,58]. Cropland was assigned to production, natural and semi-natural classes to ecology, and impervious surfaces to living. The dominant function received a weight of 0.6–1.0, larger than the

combined weight of the other two functions. Second, secondary functions received smaller weights, because a land type usually supports several functions of graded strength [37,54,59]. Examples include timber and forest products in forest, grazing in grassland and shrubland, and industrial and commercial uses within impervious surfaces. Each weight vector sums to one, so actual use forms a functional composition comparable with the closed suitability vector. The same matrix was applied to all cells and all three study years. We multiplied category area shares by these weights and summed the contributions to obtain the three actual-use functional scores. The three LANDUSE indicators are computed with the same weights (Table 1), so they equal these actual-use scores. The explanatory models therefore exclude them, together with the actual-use vector.

2.3.3. Accessibility Assessment

Transportation accessibility (ACC) represented opportunities for spatial interaction [60]. OSM roads were grouped by hierarchy and assigned ordinal relative weights according to their functional role in the road network [61–65]. Expressways and rapid roads received the highest weights, followed by national and provincial highways, arterials, and collectors (Table 3). Residential streets, service roads, and non-motorized paths received low weights. Ramps received 0.8 of the weight of their parent road class, while bus-only lanes received a moderate weight for corridor-level public transport. Because ACC is rescaled in the normalization step before TOPSIS, multiplying all weights by a constant does not change the results; only the ratios between road classes matter. The same weights were applied nationwide and in all three years, so that ACC is measured on a common scale across regions and years. ACC therefore represents road-infrastructure provision and network hierarchy.

Table 3. Functional grading and weighting settings for road types.

Road Type	Relative Weight (w)	Functional Description
Motorways and trunks	1.00	Highest-grade roads, primarily serving long-distance and high-speed transport
National/provincial roads	0.80	Arterial roads connecting major cities and regions
Secondary roads	0.60	Regional backbone roads
Tertiary roads	0.45	Subordinate corridors in urban and rural areas
Residential streets	0.25	Roads within urban residential areas
Service/unclassified roads	0.20	Roads in industrial or rural areas
Non-motorized and pedestrian paths	0.10–0.15	Pedestrian, bicycle, and farm tracks with limited contribution to transport accessibility
Connecting ramps	0.8 × parent class (0.36–0.80)	Connector segments of expressways and arterial roads
Busway	0.45	Dedicated lanes for urban public transport

Road segments were intersected with the 1 km grid, and weighted road length was divided by cell area. Distance from each cell centroid to the nearest high-level road entered a negative exponential term in the accessibility calculation:

$$ACC_i = \frac{\sum_j w_j L_{ij}}{A_i} \cdot exp\left(-\frac{d_i}{\alpha}\right) \quad (1)$$

where L_{ij} is the length of road type j within grid i (km), w_j is its assigned weight, and A_i is cell area (km^2). The distance d_i links the cell centroid to the nearest high-level road (km); α is the decay parameter, set to 5 km.

Among infrastructure-, location-, person-, and utility-based perspectives on accessibility [66], ACC is an infrastructure-based measure of road supply around each cell. Suitability-based studies of land-use conflict likewise represent accessibility by distance to roads [36,37]. Topological measures, such as intersection density, connectivity, and centrality, represent the street network as a graph of intersections and street segments [67,68]. They are typically applied to the street networks of individual cities [69]. For a national assessment at 1 km resolution, weighted density and proximity provide a measure that is consistent across urban and rural cells and across years.

ACC enters both the production and living assessments (Table 1), but its contribution differs between the two functions. Each function is evaluated separately with CRITIC–TOPSIS, so the weight of ACC depends on the other indicators of that function. In the living assessment, ACC is combined with NTL and BLD, which reflect the intensity of urban activity. Within ACC, roads of every class contribute in proportion to their length, so dense urban networks of local and collector roads yield high values. The distance term adds access to the high-level network, which serves interregional transport.

2.4. Conflict Assessment and Explanatory Modeling

We applied a common indicator system and diagnostic rules nationwide, then related the diagnostic outputs to environmental and socioeconomic indicators with XGBoost and SHAP.

2.4.1. Measurement of the Intensity of Conflicts

Using the 1 km × 1 km grid as the basic unit, we characterized the suitability structure of each cell by the vector $S = \{S_P, S_E, S_L\}$ and the actual functional structure by $A = \{A_P, A_E, A_L\}$,

where A_P, A_E, and A_L denote the functional composition of actual use, obtained by weighting CLCD area shares by the functional weights for each land-cover class (Table 2). Because the weights for each class sum to one, A is a composition. The three suitability scores, in contrast, come from separate CRITIC–TOPSIS evaluations and need not sum to one. Both vectors were therefore closed to unit sum before comparison:

$$\tilde{S}_k = \frac{S_k}{\sum S_j}, \quad \tilde{A}_k = \frac{A_k}{\sum_{j\in\{\mathrm{P,\ E,\ L}\}} A_j}, \quad k \in \{\mathrm{P,\ E,\ L}\} \tag{2}$$

$$\mathrm{CI} = \frac{1}{2} \sum_{k\in\{\mathrm{P,\ E,\ L}\}} \left|\tilde{A}_k - \tilde{S}_k\right| \tag{3}$$

The Intensity Index of Land-Use Conflicts (CI) was calculated as half the L1 distance between the two closed vectors (Equation (3)). $\tilde{S}$ describes the relative suitability structure of a cell and identifies the function for which it is comparatively most suitable. Each component is a TOPSIS relative closeness between 0 and 1, and all three are computed against the cells of the same province and year. Closure keeps the ratios between the three components and places $\tilde{S}$ on the simplex, the sample space of compositional data [70]. $\tilde{S}$ thus compares the position of a cell on the three functions within the same reference set. $\tilde{A}$ describes the functional composition of actual use. Because both vectors lie on the same three-part simplex, CI equals the total variation distance between two compositions. It ranges from 0 for identical compositions to 1 for compositions that share no functional component. CI therefore measures structural divergence between suitability and actual use. Missing suitability values from raster sampling were replaced with the provincial median

before closure. Cells in which either vector sums to zero have no defined composition. These cells (0.11% of the assessed area in each year) were excluded from CI, the direction threshold, and all statistics.

For mapping and descriptive statistics, the continuous CI values were reclassified into five ordinal levels. We used the Jenks natural breaks method to derive class boundaries from the national CI distribution and applied the same classification scheme to 2015, 2020, and 2024. The national class boundaries were CI = 0.165, 0.275, 0.376, and 0.49, separating coordination and low-, medium-, high-, and severe-intensity conflict. Natural breaks group similar CI values and separate dissimilar ones, and the method has been used to grade land-use conflict levels [36,71]. These boundaries explained more than 90% of the variance of CI in each year. The levels are ordered by CI, so a higher level denotes a larger divergence between suitability and actual use. To test sensitivity to the boundaries, class shares were recomputed with eight alternative fixed sets. These were the boundaries shifted by ±10%, Jenks breaks from each year and from all three years pooled, pooled quintiles, and equal intervals. The intensity models use the continuous CI. The lowest level is labelled coordination in the intensity classification. This label is distinct from directional coordination, which uses the provincial median CI as its threshold.

2.4.2. Classification of the Direction of Conflicts

Functional mismatch direction was defined by the ordered pair $S_{dom} \rightarrow A_{dom}$, linking the suitability-dominant function to the actual-use-dominant function within the same cell and year. Production-to-Ecology therefore denotes production-dominant suitability paired with ecology-dominant use; Ecology-to-Production denotes the reverse pairing. Dominant functions were identified as $S_{dom} = \text{argmax}_k \widetilde{S}_k$ and $A_{dom} = \text{argmax}_k \widetilde{A}_k$. Closure in Equation (2) does not change the order of the three components, so the dominant functions equal those of the raw vectors. A mismatch class was assigned when $S_{dom} \neq A_{dom}$ and CI exceeded $\tau_{p,t}$, the median CI of the valid cells in province p and year t. All other valid cells were classified as coordinated. This rule produced one coordination class and six directional mismatch classes (Table 4).

Table 4. Interpretation of the seven land-use diagnostic classes.

Diagnostic Class	Suitability-Dominant Function	Actual-Use-Dominant Function
Coordination	Matching dominant functions, or CI ≤ $\tau_{p,t}$	Matching or different; see note
Ecology-to-Production	Ecology	Production
Ecology-to-Living	Ecology	Living
Production-to-Ecology	Production	Ecology
Production-to-Living	Production	Living
Living-to-Ecology	Living	Ecology
Living-to-Production	Living	Production

Note: Directional mismatch classes require different dominant functions and CI above $\tau_{p,t}$, the median CI of the valid cells in the province and year. Coordination is assigned when the dominant functions match, or CI does not exceed $\tau_{p,t}$. The arrow implicit in each "to" label links suitability to actual use within the same cell and year; it denotes neither a temporal land-use transition nor a preferred conversion.

Directional coordination therefore has two sources: cells whose dominant functions match, and cells whose dominant functions differ but whose CI does not exceed $\tau_{p,t}$. The gate removes small divergences from the mismatch classes. Because $\tau_{p,t}$ is a within-province, within-year quantile, about half of the cells in each province and year fall at or below it. A uniform decline in CI therefore cannot by itself raise the coordinated share. Changes in that share arise from dominant-function agreement among cells above the gate. To

separate direction from the gate, we also report the ungated pairing of dominant functions for all cells.

2.4.3. Explanatory XGBoost Models

Equation (3) decomposes CI by function, whereas policy and management analysis also requires the contribution of individual indicators. Each indicator reaches CI through scaling within each province and year, CRITIC weighting, and TOPSIS, so its contribution varies among provinces and depends on the other indicators. Direction further involves the dominant-function rule and the provincial median gate. We therefore fitted explanatory XGBoost models [42] that learn the mapping from the indicators to CI and to the seven diagnostic classes. SHAP then attributed both outputs to the same predictors. The predictors were ten indicators: elevation, slope, NDVI, NPP, precipitation, nighttime light, aridity index, building density, soil pH, and soil organic carbon. The suitability and actual-use vectors were excluded. All ten predictors are suitability indicators (Table 1), so the models describe how the diagnostic outputs depend on the inputs of the indicator system.

The national models used a random sample of 200,000 cells from 2024, and each of the seven regional models used a random sample of 100,000 cells from its region. National models used a learning rate of 0.08, a maximum depth of 8, and 800 (CI) or 900 (classes) trees; regional models used XGBoost defaults with the same number of trees. The national models also used row and column subsampling rates of 0.8 (CI) or 0.85 (classes). The regional defaults were a learning rate of 0.3, a maximum depth of 6, and no subsampling. CI models used squared-error loss, class models used multiclass softmax loss, and all models used a random seed of 42. Each model was fitted to all of its sampled cells, and SHAP values were computed for the same cells.

Before fitting, values outside the valid range of each predictor were treated as missing, for example, NDVI outside −1 to 1 or building density above 1. These were mostly raster nodata codes and affected at most 0.8% of cells for any predictor. They were replaced with the national median of the predictor, so no missing values entered the models. Zero values of nighttime light and building density were kept, because they denote cells without detected light or built-up cover. XGBoost therefore treated zero as an observed value. Dependence plots summarize zero-valued inputs separately from the nonzero range.

With the same hyperparameters, the national models reached $R^2 = 0.75$ for CI and an accuracy of 0.86 (macro-F1 = 0.45; Cohen's $\kappa = 0.67$) for the seven classes on a random 20% test set. The split was stratified by class, so the models were trained on 160,000 cells and tested on 40,000 cells.

2.4.4. SHAP Interpretation of Model Associations

We applied SHapley Additive exPlanations (SHAP) to the national and regional explanatory models. Mean absolute SHAP values summarized predictor contributions to CI estimates or to the raw score for each directional class. Because the CI model and the class model have different output scales (CI units versus raw class scores), their SHAP magnitudes are not comparable. We therefore compared the two models through predictor ranks within each model and summarized the agreement between the two rankings with Spearman's ρ.

SHAP maps and summary plots described spatial variation in predictor contributions at national and regional scales. Dependence plots characterized fitted response patterns to selected predictors.

Class-specific dependence plots were derived from the national class model, using signed SHAP values for each directional class. Each plot includes all sampled cells. Predictors are displayed on their 0–1 model-input scales, and point color denotes the feature

value. Black lines connect median signed SHAP values in 50 equal-width nonzero-input bins containing at least 100 observations, and zero-valued inputs are summarized separately. SHAP values represent contributions to the raw class score, summarizing class-specific model associations.

3. Results

3.1. Production–Ecological–Living Suitability Patterns

3.1.1. Production-Space Suitability

The suitability of production space (PSS) showed an overall pattern of higher values in eastern China and lower values in western China (Figure 3a–c). The highest PSS values were concentrated in the major alluvial plains and urban agglomerations. Specifically, Jiangsu (JS, 0.849), Tianjin (TJ, 0.792), and Shandong (SD, 0.754) had relatively high PSS values in 2024. Conversely, regions such as the Qinghai–Tibet Plateau (e.g., Xizang, XZ: 0.463) and western Inner Mongolia (NM, 0.492) showed relatively low suitability levels below 0.500.

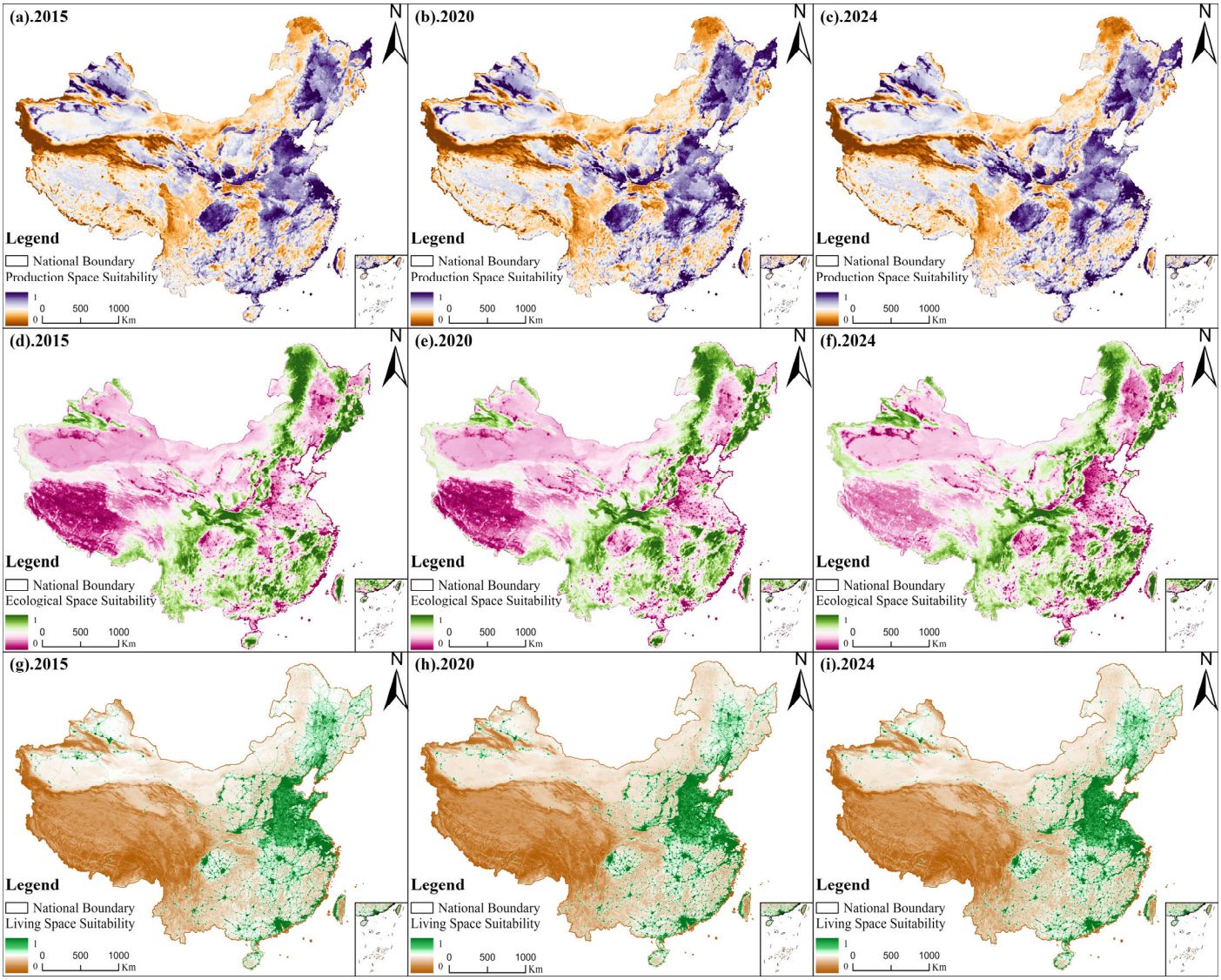


Figure 3. Suitability patterns of production, ecological, and living spaces in China for 2015, 2020, and 2024.

Temporally, PSS demonstrated regional differences in change despite a relatively stable national average (0.608 in 2015 to 0.612 in 2024). From 2015 to 2020, some inland provinces showed increases; for instance, Shanxi (SX) increased from 0.556 to 0.596. In contrast, some highly urbanized coastal regions showed slight declines or fluctuations, including Jiangsu (JS) and Tianjin (TJ) between 2015 and 2020 (e.g., JS dropped from 0.847 to 0.830). These contrasting changes in relative position within provinces indicate that a stable national mean can conceal different provincial trajectories.

3.1.2. Ecological-Space Suitability

Ecological space suitability (ESS) displayed a spatial pattern broadly contrasting with that of production space, with differences apparent across the Hu Line (Figure 3d–f). High-suitability zones were identified in the mountainous and coastal ecological barriers, with Fujian (FJ, 0.684), Taiwan (TW, 0.664), and Sichuan (SC, 0.594) ranking among the highest in 2024. In contrast, densely populated regions like the North China Plain had relatively low ecological suitability (e.g., Henan, HA: 0.370; Tianjin, TJ: 0.355).

The temporal evolution of ESS showed a decline followed by partial recovery. National mean suitability declined from 0.525 in 2015 to 0.493 in 2020, and recovered to 0.508 by 2024. The rebound did not restore national mean suitability to its initial level. Relatively low ecological suitability persisted in several metropolitan areas.

3.1.3. Living-Space Suitability

Living space suitability (LSS) presented an overall east-to-west gradient (Figure 3g–i). The highest suitability was clustered in the major coastal urban agglomerations, with Tianjin (TJ, 0.939), Jiangsu (JS, 0.876), and Shanghai (SH, 0.807) leading in 2024. Conversely, plateau and arid western provinces (e.g., Xizang, XZ and Qinghai, QH) remained at the lower end of the spectrum, with values below 0.300.

Living suitability fluctuated slightly across the three study years. The national mean decreased from 0.568 in 2015 to 0.560 in 2020, followed by a marginal recovery to 0.566 in 2024. While inland provinces such as Guizhou (GZ) maintained stable low values (~0.457), leading coastal regions like Tianjin (TJ) and Shanghai (SH) showed minimal growth or slight variations across the three years.

3.2. Intensity and Direction of Land-Use Conflicts

3.2.1. Dynamics of the Intensity of Conflicts

Across the three study years (2015, 2020, and 2024), the intensity of conflicts in China declined overall, with regional differences (Figure 4a–c). We compared conflict intensity across the three study years at national and regional scales (Figure 4d–f). The area-weighted mean CI decreased from 0.395 in 2015 to 0.385 in 2020 and 0.365 in 2024. Nationally, the combined share of medium- to severe-intensity conflicts decreased from 57.67% in 2015 to 47.33% in 2024, whereas areas with low-intensity conflicts increased from 24.06% to 29.44%, a net expansion of 514,303 km^2. Areas experiencing high-, medium-, and severe-intensity conflicts declined by 339,754 km^2, 583,470 km^2, and 64,902 km^2, respectively. Under all eight alternative boundary sets, the share of medium- to severe-intensity conflicts also declined between 2015 and 2024. For any CI threshold between 0.05 and 0.80, a smaller share of the area exceeded it in 2024 than in 2015. This national decline coexisted with regional differences: conflict intensity decreased across much of western China but remained concentrated in urbanized eastern and southern regions.

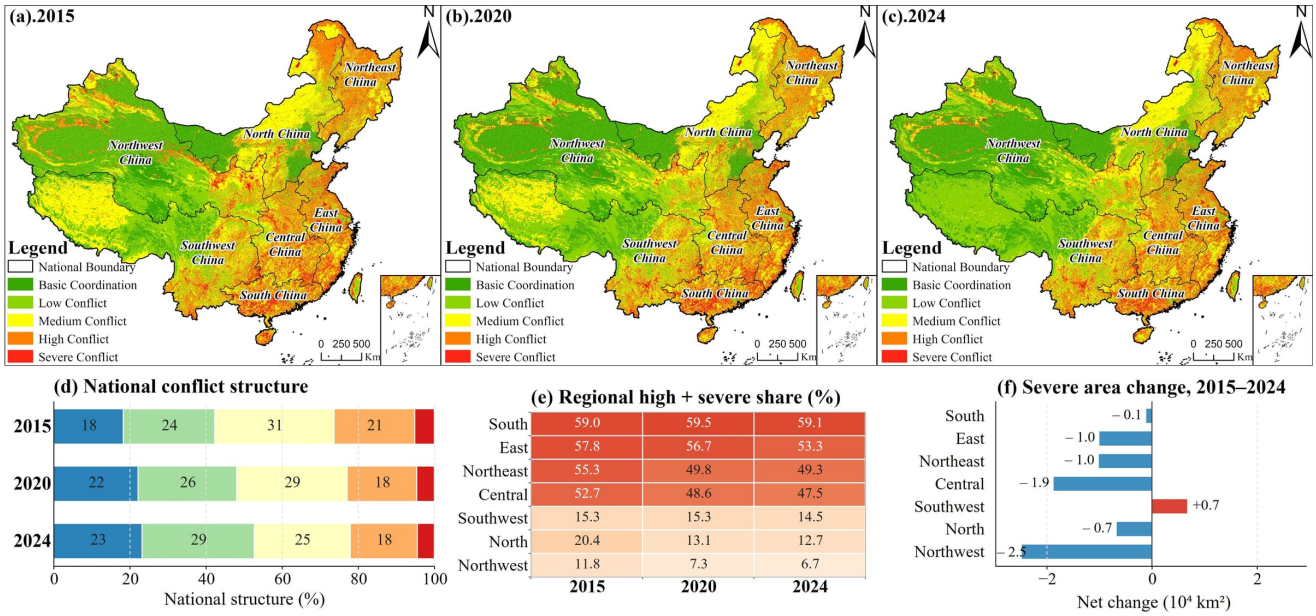


Figure 4. Dynamics of the intensity of conflicts. (**a**–**c**) Maps of the intensity of conflicts for 2015, 2020, and 2024. (**d**) National distribution of the intensity of conflicts. (**e**) Regional share of high- and severe-intensity conflicts. (**f**) Change in area experiencing severe conflicts between 2015 and 2024.

South China remained one of the regions with higher conflict intensity, with the combined share of high- and severe-intensity conflicts remaining near 59% in 2015, 2020, and 2024 (Figure 4d–f). East China declined from 57.78% to 53.31%, and Northeast China from 55.30% to 49.30%, but both remained among the regions with relatively high conflict intensity. Western regions generally had lower shares of high- and severe-intensity conflicts, with expansion of areas showing low-intensity conflicts or coordination.

3.2.2. Patterns in the Direction of Conflicts

Beyond intensity change, the directional mismatch classes indicate that the national share of coordinated cells increased, with differences among regions (Figure 5a–d). The share of coordinated cells increased from 66.68% in 2015 to 70.76% in 2024, whereas Production-to-Ecology remained the largest non-coordinated class and declined slightly from 21.32% to 20.53%. The increase in coordination thus coexisted with a persistent Production-to-Ecology component. The ungated pairing of dominant functions showed the same pattern. Without the CI gate, dominant functions differed in 49.69%, 47.75%, and 43.92% of the assessed area in 2015, 2020, and 2024. Production-to-Ecology remained the largest pairing in each year (32.59%, 32.59%, and 30.69%). Cells coordinated only because CI did not exceed the gate decreased from 16.37% to 14.67%. The rise in coordination therefore reflected greater agreement between dominant functions (50.31% to 56.08%).

Northwest and Southwest China were dominated by Production-to-Ecology mismatches, whereas East, Central, and Northeast China contained larger Living-to-Production components (Figure 5e). South China showed a more mixed combination of Production-to-Ecology, Living-to-Ecology, and Living-to-Production classes. The temporal-flow summary shows that the largest transitions between 2015 and 2024 were from Living-to-Ecology and Production-to-Ecology to coordination, together with a sizeable counter-flow from coordination to Production-to-Ecology (Figure 5f). These changes in diagnostic class membership showed that gains in coordination coexisted with new Production-to-Ecology mismatches.

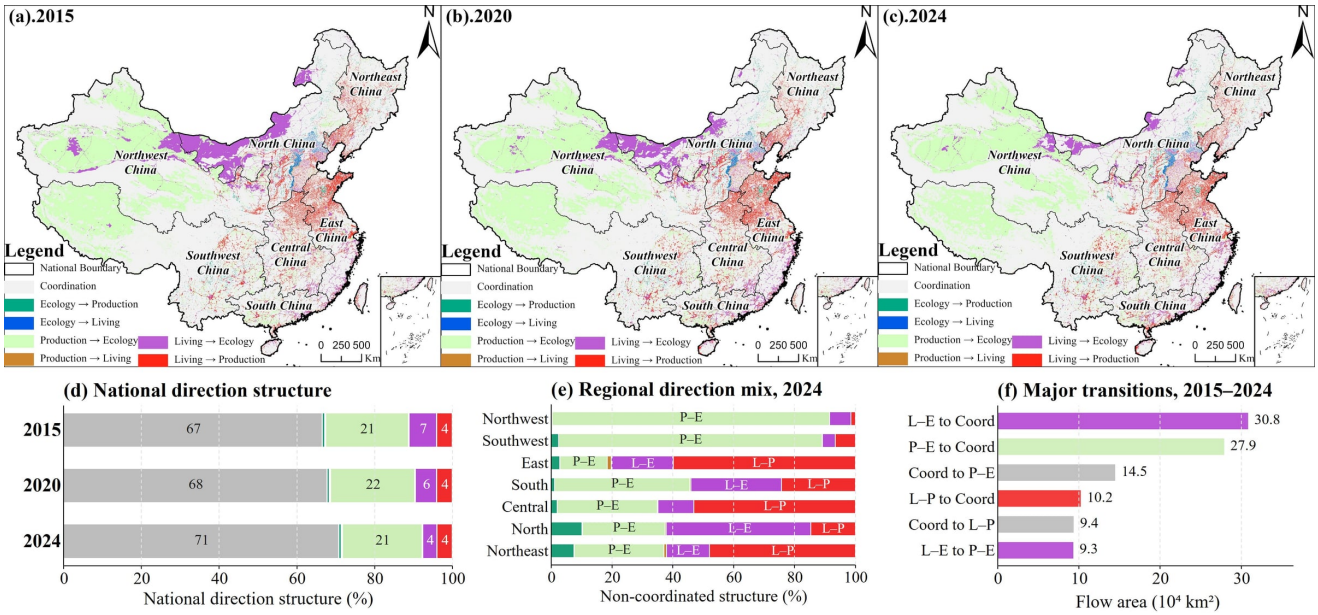


Figure 5. Patterns in the direction of conflicts. (**a**–**c**) Directional mismatch maps for 2015, 2020, and 2024. (**d**) National directional-class composition. (**e**) Regional composition of non-coordinated classes in 2024. (**f**) Major transitions among directional mismatch classes between 2015 and 2024.

3.3. Factors Associated with Land-Use Conflicts

Predictor associations varied across national and regional scales, with varying relative contributions from environmental and socioeconomic variables.

3.3.1. Factors Associated with the Intensity of Conflicts

At the national scale, the intensity of conflicts was associated mainly with terrain, vegetation, and hydroclimatic variables (Figure 6a). Elevation (mean |SHAP| = 0.034; 20.3%) and NDVI (0.034; 20.0%) contributed most, followed by slope (0.025; 14.6%) and precipitation (0.024; 14.2%). Across the seven regions, terrain, vegetation, and water-availability variables likewise occupied the leading ranks in the intensity model (Figure 7a).

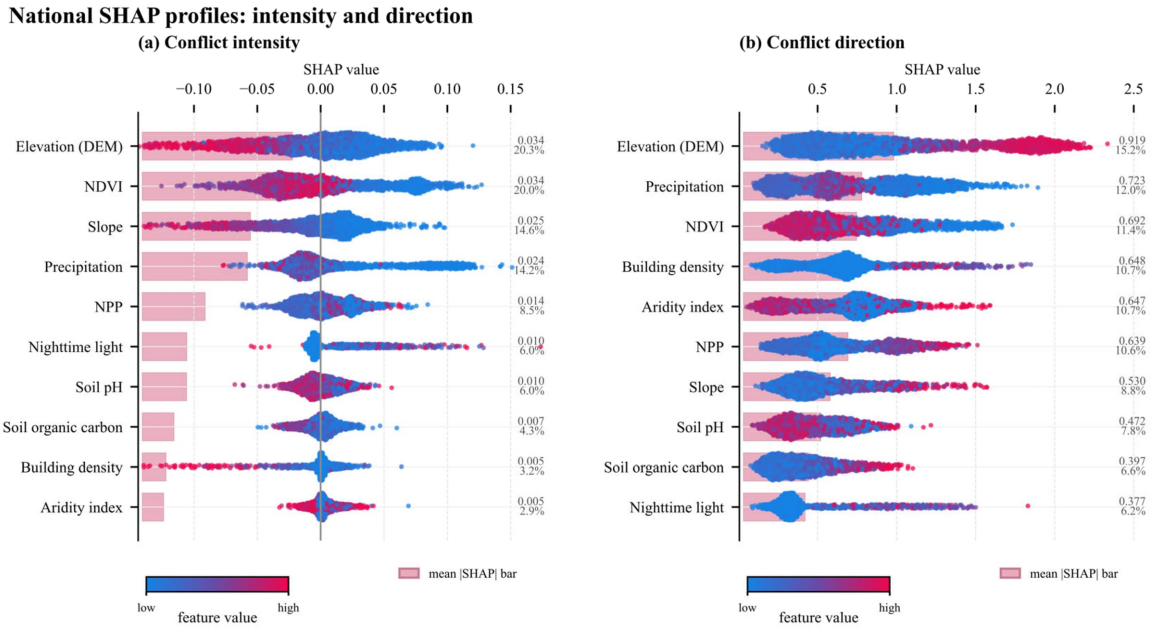


Figure 6. National SHAP profiles for (**a**) intensity of conflicts and (**b**) direction of conflicts.

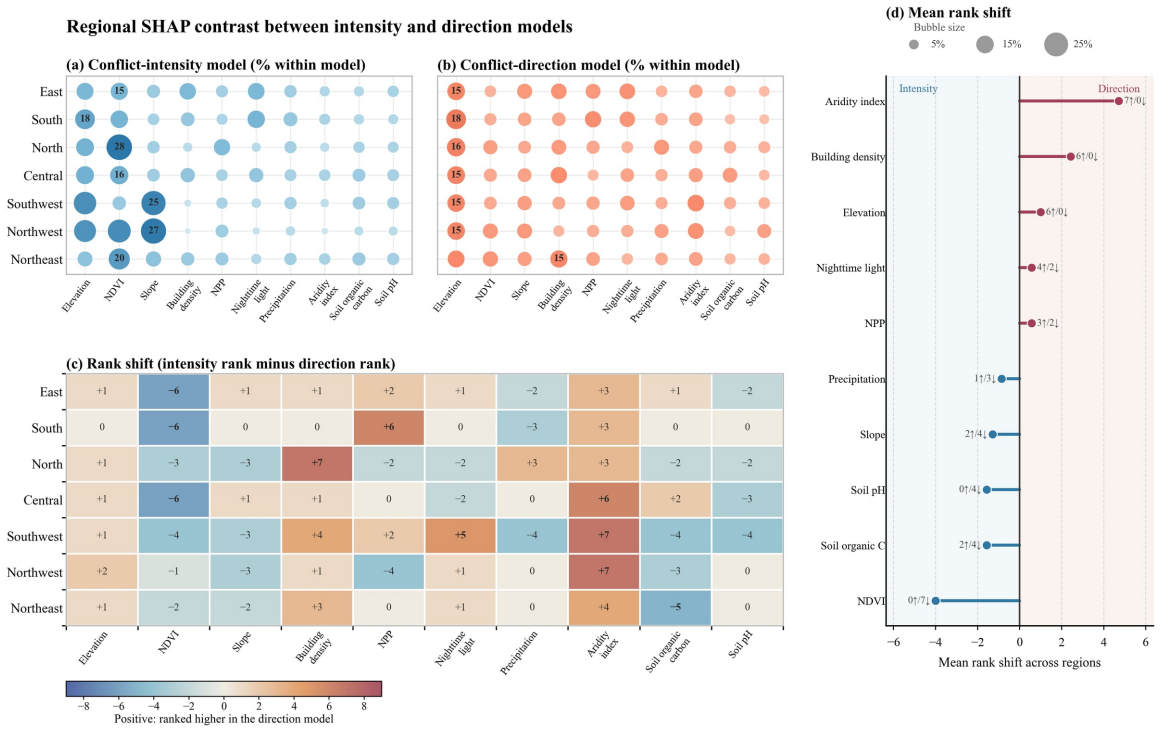


Figure 7. Regional SHAP contrast between the intensity and direction models. (**a**,**b**) Within-model contribution shares (%) for the intensity and direction models. (**c**) Rank shift, defined as the rank of each predictor in the intensity model minus its rank in the direction model; positive values indicate a higher rank in the direction model. (**d**) Mean rank shift across the seven regions, with the number of regions showing an upward or downward shift.

3.3.2. Factors Associated with the Direction of Conflicts

At the national level, the direction of conflicts was most strongly associated with elevation, precipitation, vegetation condition, and development intensity (Figure 6b). Elevation had the largest contribution (mean |SHAP| = 0.919; 15.2%), followed by precipitation (0.723; 12.0%), NDVI (0.692; 11.4%), building density (0.648; 10.7%), and aridity index (0.647; 10.7%).

Predictor rankings differed systematically between the direction and intensity models (Figure 7a,b). Nationally, building density moved from ninth in the intensity model to fourth in the direction model, and aridity from tenth to fifth (Figure 6). Across regions, elevation ranked first in the direction model in six regions, whereas building density ranked first in Northeast China (Figure 7b). Aridity ranked higher in the direction model than in the intensity model in all seven regions, and building density ranked higher in six, with no change in South China (Figure 7c,d). Conversely, NDVI ranked lower in the direction model in all seven regions, and slope ranked lower in four. Rank agreement between the two models was moderate nationally (Spearman's $\rho = 0.45$) and absent in Southwest China ($\rho = -0.02$), indicating that intensity and direction draw on different predictors within the indicator system.

Building density and aridity both ranked higher in the direction model, and their SHAP contributions varied across coordination and three mismatch classes (Figure 8). Increasing building density was associated with predominantly negative SHAP contributions to Production-to-Ecology (Figure 8b). By contrast, Living-to-Production showed positive contributions across low-to-intermediate nonzero densities, while Living-to-Ecology shifted from positive to negative contributions at higher densities (Figure 8c,d). Along the aridity input scale, contributions to Living-to-Production changed from strongly negative to positive, whereas contributions to coordination remained comparatively small (Figure 8e,g).

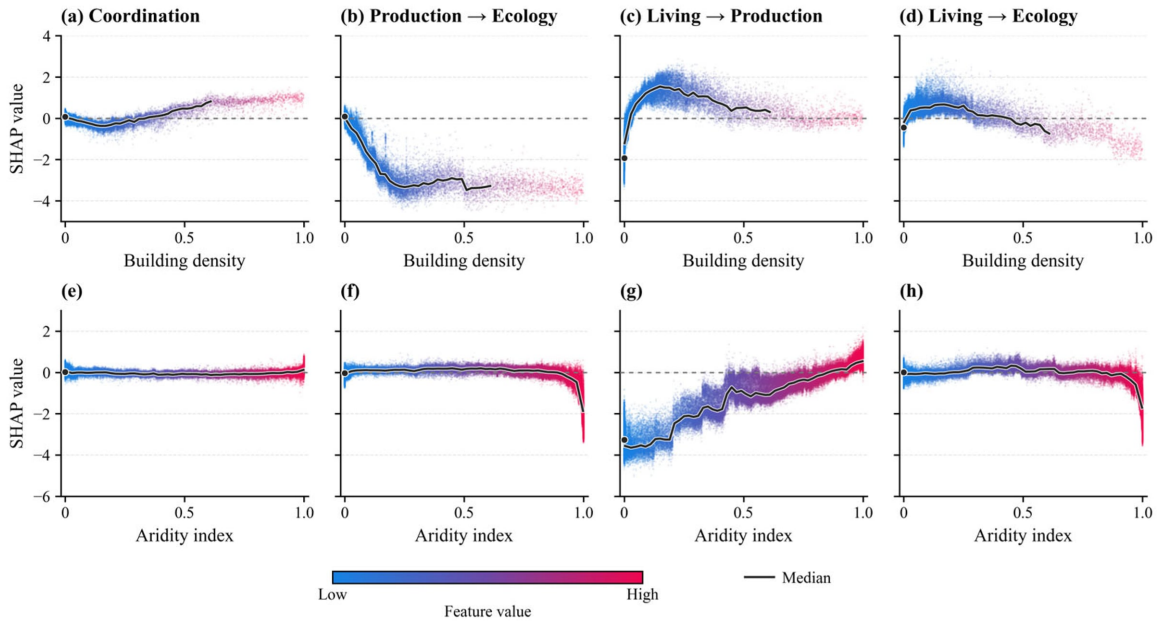


Figure 8. Class-specific SHAP responses to building density and aridity index: (**a**) building density and Coordination; (**b**) building density and Production-to-Ecology; (**c**) building density and Living-to-Production; (**d**) building density and Living-to-Ecology; (**e**) aridity index and Coordination; (**f**) aridity index and Production-to-Ecology; (**g**) aridity index and Living-to-Production; (**h**) aridity index and Living-to-Ecology.

4. Discussion

4.1. Functional Mismatch Patterns and Implications for Differentiated Land Management

Direction identifies the functional relationship underlying each suitability–use mismatch. Zong et al. [31] distinguished potential conflict types through combinations of land suitability and quantified their intensity and change. Here, direction links the suitability-dominant function to the actual-use-dominant function. It separates Production-to-Ecology from Ecology-to-Production, which involve the same two functions but different suitability–use relationships. Nationally, moderate-to-severe conflicts declined from 57.67% to 47.33%, whereas Production-to-Ecology remained widespread, changing from 21.32% to 20.53%. Regionally, Production-to-Ecology dominated Northwest and Southwest China, whereas East, Central, and Northeast China contained larger Living-to-Production components. South China combined Production-to-Ecology, Living-to-Ecology, and Living-to-Production classes. This direction thus reveals persistent mismatches behind the declining intensity trend, and each class raises a different question for land management.

Each mismatch class indicates what local verification should examine. In Production-to-Ecology areas, verification should compare production-suitability assumptions with existing ecological functions and conservation requirements. On the Qinghai–Tibet Plateau, these requirements include the conservation value of alpine vegetation. Ecological use may remain appropriate even where the model assigns higher production suitability. In Living-to-Production and Living-to-Ecology areas, verification should compare conditions underlying living suitability with current agricultural or ecological value, housing and service demand, and planning constraints such as farmland protection. The coexistence of efficiency benefits and ecological costs reported for urban form–function compactness [40] further supports weighing multiple outcomes before acting on a diagnostic category. Combined with independent evidence of land-use change and occupancy, the class-specific SHAP responses indicate which conditions to examine first.

The appropriate response to a verified mismatch depends on whether it reflects a protection decision or an unplanned divergence between suitability and use. Overlaying the mismatch maps on ecological protection red lines and permanent basic farmland [20] makes this distinction. Inside these zones, the response is to retain the current use and manage its costs and development pressures. Where Production-to-Ecology mismatches in Northwest and Southwest China lie under protection, ecological compensation can offset the forgone production. China's Grassland Ecological Compensation Policy, for example, raised herders' incomes and modestly improved grassland quality [72]. Where Living-to-Production mismatches in East, Central, and Northeast China lie on protected farmland, development demand can be directed into urban development boundaries. Planning controls can hold development back from such land: in Fujian, the Major Function Oriented Zone plan prevented 79.31 km^2 of built-up land in development-restricted zones during 2013–2020 [73]. Mismatches outside protected zones are candidates for adjustment. Zoning can guide this adjustment: combining conflict status with ecological quality, a basin study defined six control zones, including priority-treatment and development-potential zones [74]. Scenario simulation can test responses before implementation: in the Beijing–Tianjin–Hebei region, projected conflicts eased under an ecological-security scenario but intensified under business-as-usual and cropland-protection scenarios [17]. Stakeholder participation can also change the selected option: participatory and expert-led prioritizations of nature-based solutions diverged in northern Tanzania [75]. The national screening thus indicates which cells to examine and which responses to consider, and local data on tenure, demand, and stakeholder priorities guide the final choice.

4.2. Contrasting Associations of Conflict Intensity and Functional Mismatch Direction

The distinction between conflict intensity and functional mismatch direction extends beyond differences in variable importance to differences in how individual variables relate to specific mismatch classes. Building density ranked fourth among the ten predictors in the direction model but ninth in the intensity model, and aridity ranked fifth and tenth, respectively (Figure 6). Yet environmental variables remained prominent in both models. These findings show that the conditions associated with mismatch magnitude differ from those associated with its functional configuration, making class-specific response analysis essential.

Building density provides the clearest illustration of this distinction. Its contributions were predominantly negative for Production-to-Ecology but positive for Living-to-Production at low-to-intermediate densities. Development-related conditions thus separate particular suitability–use relationships. A similar contrast appears in the national pattern reported by Zong et al. [31]: agriculture–construction conflict occurred mainly in the eastern plains, and agriculture–ecology conflict mainly in the west. City-scale studies likewise located construction–agricultural conflict near the city center [71] and strong conflicts in urban–rural transition zones [36]. Consequently, the higher directional rank of building density reflects its role in differentiating functional mismatch types.

This differentiation also occurred among environmental variables, such as aridity, and across regions. In Northwest China, aridity ranked second in the direction model but ninth in the intensity model, whereas slope ranked first in the intensity model and fourth in the direction model (Figure 7). Environmental conditions thus act differently on mismatch magnitude and on the specific functional relationship involved.

Together, these results show why intensity and direction should be interpreted jointly. Intensity identifies the magnitude of suitability–use divergence, whereas class-specific associations characterize the conditions under which different functional configurations occur.

4.3. Contributions, Limitations, and Future Directions

The central contribution is a joint assessment of conflict intensity and functional mismatch direction within a common suitability–use framework. Intensity quantifies the size of the discrepancy, while direction preserves the ordered relationship between the two dominant functions. Their combined interpretation shows how declining intensity can coexist with persistent functional mismatches. Class-specific SHAP responses extend this diagnosis by identifying differing model associations among directional classes.

Differences in the spatial resolution of the source datasets introduce uncertainty into the grid-based analysis. Although the 30 m land-cover data retain information on class composition within each 1 km cell, aggregation does not preserve the detailed spatial arrangement of those classes. Resampling continuous variables can smooth local extremes and spatial gradients, potentially affecting suitability estimates and the classification of cells close to conflict-intensity thresholds. Future work should compare alternative grid sizes and resampling schemes to assess the sensitivity of conflict intensity, functional direction, and their temporal changes to spatial scale.

Three additional limitations should be noted. First, the 1 km resolution cannot capture sub-kilometer urban features that likely shape the dynamics of conflicts in dense metropolitan cores. These features include building height, mixed-use zoning, and street-level accessibility, such as intersection density and network connectivity. Second, the SHAP patterns of the explanatory models describe associations within the sampled data. Because their predictors are also suitability indicators, these patterns are attributions within the indicator system rather than evidence of independent drivers. Third, we did not report uncertainty intervals for the SHAP shares and rank differences (Figures 6 and 7), so small differences among them may reflect sampling noise.

The diagnostic framework also depends on indicator selection, land-cover-to-function weights, road-class weights, and dominant-function classification. A nationwide indicator system improves procedural consistency but cannot fully represent local farming practices, mixed land uses, conservation objectives, or institutional constraints. Because land cover contributes to both suitability assessment and actual-use representation, the two sides are not wholly independent. BLD and NTL are also state proxies rather than direct observations of functional demand. The mapped mismatches should therefore be interpreted as screening results conditional on the adopted assumptions.

The assessed suitability is a reference constructed from chosen indicators and weights, not an objective property of land. In multi-criteria evaluation, weights reflect the decision-makers as much as the criteria, and data-derived weights gain replicability but capture little preference information [76]. Our CRITIC weights are data-derived, so they do not encode policy objectives. The indicators, however, embed earlier decisions: planned main roads in Shenzhen's master plan, for example, influenced its urban growth patterns [77]. ACC therefore carries past planning choices into production and living suitability. In China, carrying-capacity and suitability evaluations form the basis of territorial spatial planning, which delimits ecological protection red lines, permanent basic farmland, and urban development boundaries [20]. Some suitability assessments include planning designations, such as basic farmland protection areas and nature reserves, as indicators [78], whereas ours does not. Land uses that follow these designations can therefore appear as mismatches: conservation can keep production-suitable land in ecological use, and farmland protection can keep land near settlements in production. These Production-to-Ecology and Living-to-Production mismatches mark where policy has assigned a use other than the one the indicators favor. Whether such a mismatch calls for action depends on the objectives that the policy serves.

Future research should prioritize two directions. First, higher-frequency earth observation can be coupled with socioeconomic sensing and policy-event data to move from cross-sectional snapshots toward continuous monitoring. Second, diagnostic outputs can be linked to agent-based or participatory simulation so that model-derived response ranges can be tested under alternative governance scenarios.

5. Conclusions

This study developed a direction-aware framework for diagnosing land-use conflicts by distinguishing the magnitude of suitability–use mismatch from its functional direction. Applied to China at a 1 km resolution for 2015, 2020, and 2024, the framework revealed a broad decline in conflict intensity, with the share of moderate-to-severe conflicts decreasing from 57.67% to 47.33%. This overall improvement, however, was spatially uneven: conflict pressure declined more markedly in western China, while high- and severe-intensity conflicts remained concentrated in the south and east. At the same time, the share of coordinated cells increased from 66.68% to 70.76%, but Production-to-Ecology remained the dominant mismatch class, declining only slightly from 21.32% to 20.53%. Northwest and Southwest China were characterized mainly by Production-to-Ecology mismatches, whereas East, Central, and Northeast China contained larger Living-to-Production components.

The analysis further showed that conflict intensity and functional mismatch direction were associated with different combinations of environmental and socioeconomic conditions. Terrain, vegetation, and hydroclimatic variables ranked highest in the intensity model, whereas building density and aridity ranked consistently higher in the direction model than in the intensity model. More importantly, these associations were class-specific rather than uniform. Building density was negatively associated with Production-to-Ecology but positively associated with Living-to-Production across low-to-intermediate nonzero densities, while aridity also showed contrasting responses among directional classes. These results indicate that the factors associated with where conflicts are severe are not necessarily the same as those associated with how conflicts are functionally expressed.

Joint assessment of intensity and direction distinguishes the magnitude of suitability–use divergence from the functional relationship involved. The persistent Production-to-Ecology component shows why declining intensity alone provides an incomplete account of functional alignment. These paired outputs provide a basis for regional comparison and targeted examination of suitability assumptions, existing functions, and protection requirements.

Author Contributions: Conceptualization, Wenxu Wu; methodology, Peng Ti, Hong Chen and Yining Zhang; software, Hongguo Jia; formal analysis, Wenxu Wu and Yong Dong; resources, Yong Dong; writing—original draft preparation, Wenxu Wu; writing—review and editing, Peng Ti, Hong Chen, Hongguo Jia and Yining Zhang; visualization, Wenxu Wu, Hong Chen and Hongguo Jia; supervision, Peng Ti; project administration, Peng Ti and Yong Dong. All authors have read and agreed to the published version of the manuscript.

Funding: This research was funded by the Science and Technology Department of Sichuan Province, grant numbers 2025ZNSFSC0325 and 2025ZNSFSC0330.

Data Availability Statement: The data and code supporting the findings of this study are available from the corresponding author upon reasonable request.

Acknowledgments: The authors thank the editors and anonymous reviewers for their constructive comments.

Conflicts of Interest: The authors declare no conflicts of interest.

References

1. Meyfroidt, P.; de Bremond, A.; Ryan, C.M.; Archer, E.; Aspinall, R.; Chhabra, A.; Camara, G.; Corbera, E.; DeFries, R.; Díaz, S.; et al. Ten facts about land systems for sustainability. *Proc. Natl. Acad. Sci. USA* **2022**, *119*, e2109217118. [CrossRef] [PubMed]
2. Bergstrom, J.C.; Goetz, S.J.; Shortle, J.S. *Land Use Problems and Conflicts: Causes, Consequences and Solutions*; Routledge: London, UK, 2004. [CrossRef]
3. van Dijk, M.; Morley, T.; Rau, M.L.; Saghai, Y. A meta-analysis of projected global food demand and population at risk of hunger for the period 2010–2050. *Nat. Food* **2021**, *2*, 494–501. [CrossRef] [PubMed]
4. Gao, J.; O'Neill, B.C. Mapping global urban land for the 21st century with data-driven simulations and Shared Socioeconomic Pathways. *Nat. Commun.* **2020**, *11*, 2302. [CrossRef] [PubMed]
5. Potapov, P.; Turubanova, S.; Hansen, M.C.; Tyukavina, A.; Zalles, V.; Khan, A.; Song, X.-P.; Pickens, A.; Shen, Q.; Cortez, J. Global maps of cropland extent and change show accelerated cropland expansion in the twenty-first century. *Nat. Food* **2022**, *3*, 19–28. [CrossRef] [PubMed]
6. Song, X.-P.; Hansen, M.C.; Potapov, P.; Adusei, B.; Pickering, J.; Adami, M.; Lima, A.; Zalles, V.; Stehman, S.V.; Di Bella, C.M.; et al. Massive soybean expansion in South America since 2000 and implications for conservation. *Nat. Sustain.* **2021**, *4*, 784–792. [CrossRef] [PubMed]
7. Bousfield, C.G.; Morton, O.; Edwards, D.P. Climate change will exacerbate land conflict between agriculture and timber production. *Nat. Clim. Change* **2024**, *14*, 1071–1077. [CrossRef]
8. Hoang, N.T.; Taherzadeh, O.; Ohashi, H.; Yonekura, Y.; Nishijima, S.; Yamabe, M.; Matsui, T.; Matsuda, H.; Moran, D.; Kanemoto, K. Mapping potential conflicts between global agriculture and terrestrial conservation. *Proc. Natl. Acad. Sci. USA* **2023**, *120*, e2208376120. [CrossRef] [PubMed]
9. Huang, Q.; Liu, Z.; He, C.; Gou, S.; Bai, Y.; Wang, Y.; Shen, M. The occupation of cropland by global urban expansion from 1992 to 2016 and its implications. *Environ. Res. Lett.* **2020**, *15*, 084037. [CrossRef]
10. Bren d'Amour, C.; Reitsma, F.; Baiocchi, G.; Barthel, S.; Güneralp, B.; Erb, K.-H.; Haberl, H.; Creutzig, F.; Seto, K.C. Future urban land expansion and implications for global croplands. *Proc. Natl. Acad. Sci. USA* **2017**, *114*, 8939–8944. [CrossRef] [PubMed]
11. van Vliet, J. Direct and indirect loss of natural area from urban expansion. *Nat. Sustain.* **2019**, *2*, 755–763. [CrossRef]
12. Kleemann, J.; Struve, B.; Spyra, M. Conflicts in urban peripheries in Europe. *Land Use Policy* **2023**, *133*, 106849. [CrossRef]
13. Narducci, J.; Quintas-Soriano, C.; Castro, A.; Som-Castellano, R.; Brandt, J.S. Implications of urban growth and farmland loss for ecosystem services in the western United States. *Land Use Policy* **2019**, *86*, 1–11. [CrossRef]
14. Grădinaru, S.R.; Paraschiv, M.; Iojă, C.I.; van Vliet, J. Conflicting interests between local governments and the European target of no net land take. *Environ. Sci. Policy* **2023**, *142*, 1–11. [CrossRef]
15. Liu, Y.; Zhou, Y. Reflections on China's food security and land use policy under rapid urbanization. *Land Use Policy* **2021**, *109*, 105699. [CrossRef]
16. Yang, L.; Fang, C.; Chen, W.; Zeng, J. Urban-rural land structural conflicts in China: A land use transition perspective. *Habitat Int.* **2023**, *138*, 102877. [CrossRef]
17. Bao, W.; Yang, Y.; Zou, L. How to reconcile land use conflicts in mega urban agglomeration? A scenario-based study in the Beijing-Tianjin-Hebei region, China. *J. Environ. Manag.* **2021**, *296*, 113168. [CrossRef] [PubMed]
18. Wu, W.; Zhou, L.; Wang, S.; Wei, W.; Chen, Z.; Zhang, Q.; Wang, W. Identification of urban fringe areas and assessment of their landscape ecological risks in Xi'an, China. *Chin. Geogr. Sci.* **2025**, *35*, 1013–1029. [CrossRef]
19. Bryan, B.A.; Gao, L.; Ye, Y.; Sun, X.; Connor, J.D.; Crossman, N.D.; Stafford-Smith, M.; Wu, J.; He, C.; Yu, D.; et al. China's response to a national land-system sustainability emergency. *Nature* **2018**, *559*, 193–204. [CrossRef] [PubMed]
20. Liu, Y.; Zhou, Y. Territory spatial planning and national governance system in China. *Land Use Policy* **2021**, *102*, 105288. [CrossRef]
21. Chen, M.; Gong, Y.; Li, Y.; Lu, D.; Zhang, H. Population distribution and urbanization on both sides of the Hu Huanyong Line: Answering the Premier's question. *J. Geogr. Sci.* **2016**, *26*, 1593–1610. [CrossRef]
22. Chen, D.; Zhang, Y.; Yao, Y.; Hong, Y.; Guan, Q.; Tu, W. Exploring the spatial differentiation of urbanization on two sides of the Hu Huanyong Line—Based on nighttime light data and cellular automata. *Appl. Geogr.* **2019**, *112*, 102081. [CrossRef]
23. Kong, X.; Fu, M.; Zhao, X.; Wang, J.; Jiang, P. Ecological effects of land-use change on two sides of the Hu Huanyong Line in China. *Land Use Policy* **2022**, *113*, 105895. [CrossRef]
24. Brown, G.; Raymond, C.M. Methods for identifying land use conflict potential using participatory mapping. *Landsc. Urban Plan.* **2014**, *122*, 196–208. [CrossRef]
25. Lin, Q.; Tan, S.; Zhang, L.; Wang, S.; Wei, C.; Li, Y. Conflicts of land expropriation in China during 2006–2016: An overview and its spatio-temporal characteristics. *Land Use Policy* **2018**, *76*, 246–251. [CrossRef]
26. Steinhäußer, R.; Siebert, R.; Steinführer, A.; Hellmich, M. National and regional land-use conflicts in Germany from the perspective of stakeholders. *Land Use Policy* **2015**, *49*, 183–194. [CrossRef]
27. Fienitz, M.; Siebert, R. Latent, collaborative, or escalated conflict? Determining causal pathways for land use conflicts. *Land Use Policy* **2023**, *134*, 106918. [CrossRef]

28. Bekele, A.E.; Drabik, D.; Dries, L.; Heijman, W. Large-scale land investments and land-use conflicts in the agro-pastoral areas of Ethiopia. *Land Use Policy* **2022**, *119*, 106166. [CrossRef]
29. Cegielska, K.; Różycka-Czas, R.; Gorzelany, J.; Olczak, B. Land use and land cover conflict risk assessment model: Social and spatial impact of suburbanisation. *Landsc. Urban Plan.* **2025**, *257*, 105302. [CrossRef]
30. Jiang, S.; Meng, J.; Zhu, L.; Cheng, H. Spatial-temporal pattern of land use conflict in China and its multilevel driving mechanisms. *Sci. Total Environ.* **2021**, *801*, 149697. [CrossRef] [PubMed]
31. Zong, S.; Xu, S.; Jiang, X.; Song, C. Identification and dynamic evolution of land use conflict potentials in China, 2000–2020. *Ecol. Indic.* **2024**, *166*, 112340. [CrossRef]
32. Zabel, F.; Delzeit, R.; Schneider, J.M.; Seppelt, R.; Mauser, W.; Václavík, T. Global impacts of future cropland expansion and intensification on agricultural markets and biodiversity. *Nat. Commun.* **2019**, *10*, 2844. [CrossRef] [PubMed]
33. Rehbein, J.A.; Watson, J.E.M.; Lane, J.L.; Sonter, L.J.; Venter, O.; Atkinson, S.C.; Allan, J.R. Renewable energy development threatens many globally important biodiversity areas. *Glob. Change Biol.* **2020**, *26*, 3040–3051. [CrossRef] [PubMed]
34. Cieślak, I. Identification of areas exposed to land use conflict with the use of multiple-criteria decision-making methods. *Land Use Policy* **2019**, *89*, 104225. [CrossRef]
35. Luo, K.; Samat, A.; Du, P.; Liu, S.; Liang, J.; Abuduwaili, J.; Shokparova, D.; Juliev, M. Integrative analysis of transboundary land use conflicts in the Aral Sea Basin: A multi-scale assessment of drivers and strategies for sustainable management. *Resour. Environ. Sustain.* **2025**, *21*, 100240. [CrossRef]
36. Dong, G.; Ge, Y.; Jia, H.; Sun, C.; Pan, S. Land use multi-suitability, land resource scarcity and diversity of human needs: A new framework for land use conflict identification. *Land* **2021**, *10*, 1003. [CrossRef]
37. Lin, G.; Fu, J.; Jiang, D. Production–living–ecological conflict identification using a multiscale integration model based on spatial suitability analysis and sustainable development evaluation: A case study of Ningbo, China. *Land* **2021**, *10*, 383. [CrossRef]
38. Han, B.; Jin, X.; Zhao, Q.; Chen, H. Spatiotemporal patterns and mechanisms of land-use conflicts affecting high-quality development in China. *Appl. Geogr.* **2023**, *155*, 102972. [CrossRef]
39. Wang, D.; Wang, M.; Zheng, W.; Song, Y.; Huang, X. A multi-level spatial assessment framework for identifying land use conflict zones. *Land Use Policy* **2025**, *148*, 107382. [CrossRef]
40. Xu, Z.; Lan, T.; Wu, Y.; Yan, J.; Tang, L. Quantifying environmental trade-offs of urban form-function compactness. *Environ. Res. Lett.* **2026**, *21*, 044011. [CrossRef]
41. Jiang, Y.; Zhou, L.; Wang, B.; Zhang, Q.; Gao, H.; Wang, S.; Cui, M. The impact of gradient expansion of urban–rural construction land on landscape fragmentation in typical mountain cities, China. *Int. J. Digit. Earth* **2024**, *17*, 2310093. [CrossRef]
42. Chen, T.; Guestrin, C. XGBoost: A scalable tree boosting system. In *Proceedings of the 22nd ACM SIGKDD International Conference on Knowledge Discovery and Data Mining, San Francisco, CA, USA, 13–17 August 2016*; Association for Computing Machinery: New York, NY, USA, 2016; pp. 785–794. [CrossRef]
43. Xiao, J. Calculating the Hu Huanyong Line. *Ann. Am. Assoc. Geogr.* **2026**, *116*, 17–38. [CrossRef]
44. Yang, J.; Huang, X. The 30 m annual land cover dataset and its dynamics in China from 1990 to 2019. *Earth Syst. Sci. Data* **2021**, *13*, 3907–3925. [CrossRef]
45. Fick, S.E.; Hijmans, R.J. WorldClim 2: New 1-km spatial resolution climate surfaces for global land areas. *Int. J. Climatol.* **2017**, *37*, 4302–4315. [CrossRef]
46. Zomer, R.J.; Xu, J.; Trabucco, A. Version 3 of the Global Aridity Index and Potential Evapotranspiration Database. *Sci. Data* **2022**, *9*, 409. [CrossRef] [PubMed]
47. Poggio, L.; de Sousa, L.M.; Batjes, N.H.; Heuvelink, G.B.M.; Kempen, B.; Ribeiro, E.; Rossiter, D. SoilGrids 2.0: Producing soil information for the globe with quantified spatial uncertainty. *Soil* **2021**, *7*, 217–240. [CrossRef]
48. Wu, Y.; Shi, K.; Chen, Z.; Liu, S.; Chang, Z. Developing Improved Time-Series DMSP-OLS-Like Data (1992–2019) in China by Integrating DMSP-OLS and SNPP-VIIRS. *IEEE Trans. Geosci. Remote Sens.* **2022**, *60*, 4407714. [CrossRef]
49. Xu, Z.; Xu, G.; Lan, T.; Li, X.; Chen, Z.; Cui, H.; Zhou, Z.; Wang, H.; Jiao, L.; Small, C. Global consistency of urban scaling evidenced by remote sensing. *PNAS Nexus* **2025**, *4*, pgaf037. [CrossRef] [PubMed]
50. Du, X.; Wang, Y.; Chen, F. Evaluation of coal-resource-based cities transformation based on CRITIC-TOPSIS model. *Sustain. Cities Soc.* **2024**, *103*, 105271. [CrossRef]
51. Çelikbilek, Y.; Tüysüz, F. An in-depth review of theory of the TOPSIS method: An experimental analysis. *J. Manag. Anal.* **2020**, *7*, 281–300. [CrossRef]
52. Burkhard, B.; Kroll, F.; Nedkov, S.; Müller, F. Mapping ecosystem service supply, demand and budgets. *Ecol. Indic.* **2012**, *21*, 17–29. [CrossRef]
53. Jacobs, S.; Burkhard, B.; Van Daele, T.; Staes, J.; Schneiders, A. 'The Matrix Reloaded': A review of expert knowledge use for mapping ecosystem services. *Ecol. Model.* **2015**, *295*, 21–30. [CrossRef]
54. Liu, J.; Liu, Y.; Li, Y. Classification evaluation and spatial-temporal analysis of "production-living-ecological" spaces in China. *Acta Geogr. Sin.* **2017**, *72*, 1290–1304. [CrossRef]

55. Kong, D.; Chen, H.; Wu, K. The evolution of "Production-Living-Ecological" space, eco-environmental effects and its influencing factors in China. *J. Nat. Resour.* **2021**, *36*, 1116–1135. [CrossRef]
56. Lin, G.; Jiang, D.; Fu, J.; Zhao, Y. A review on the overall optimization of production–living–ecological space: Theoretical basis and conceptual framework. *Land* **2022**, *11*, 345. [CrossRef]
57. Zhang, R.; Li, S.; Wei, B.; Zhou, X. Characterizing production–living–ecological space evolution and its driving factors: A case study of the Chaohu Lake Basin in China from 2000 to 2020. *ISPRS Int. J. Geo-Inf.* **2022**, *11*, 447. [CrossRef]
58. Fu, J.; Gao, Q.; Jiang, D.; Li, X.; Lin, G. Spatial–temporal distribution of global production–living–ecological space during the period 2000–2020. *Sci. Data* **2023**, *10*, 589. [CrossRef] [PubMed]
59. Verburg, P.H.; van de Steeg, J.; Veldkamp, A.; Willemen, L. From land cover change to land function dynamics: A major challenge to improve land characterization. *J. Environ. Manag.* **2009**, *90*, 1327–1335. [CrossRef] [PubMed]
60. Hansen, W.G. How Accessibility Shapes Land Use. *J. Am. Inst. Plan.* **1959**, *25*, 73–76. [CrossRef]
61. Rose, N.; Cowie, C.; Gillett, R.; Marks, G.B. Weighted road density: A simple way of assigning traffic-related air pollution exposure. *Atmos. Environ.* **2009**, *43*, 5009–5014. [CrossRef]
62. Venter, O.; Sanderson, E.W.; Magrach, A.; Allan, J.R.; Beher, J.; Jones, K.R.; Possingham, H.P.; Laurance, W.F.; Wood, P.; Fekete, B.M.; et al. Global terrestrial Human Footprint maps for 1993 and 2009. *Sci. Data* **2016**, *3*, 160067. [CrossRef] [PubMed]
63. Weiss, D.J.; Nelson, A.; Gibson, H.S.; Temperley, W.; Peedell, S.; Lieber, A.; Hancher, M.; Poyart, E.; Belchior, S.; Fullman, N.; et al. A global map of travel time to cities to assess inequalities in accessibility in 2015. *Nature* **2018**, *553*, 333–336. [CrossRef] [PubMed]
64. Nelson, A.; Weiss, D.J.; van Etten, J.; Cattaneo, A.; McMenomy, T.S.; Koo, J. A suite of global accessibility indicators. *Sci. Data* **2019**, *6*, 266. [CrossRef] [PubMed]
65. Meijer, J.R.; Huijbregts, M.A.J.; Schotten, K.C.G.J.; Schipper, A.M. Global patterns of current and future road infrastructure. *Environ. Res. Lett.* **2018**, *13*, 064006. [CrossRef]
66. Geurs, K.T.; van Wee, B. Accessibility evaluation of land-use and transport strategies: Review and research directions. *J. Transp. Geogr.* **2004**, *12*, 127–140. [CrossRef]
67. Porta, S.; Crucitti, P.; Latora, V. The network analysis of urban streets: A primal approach. *Environ. Plan. B Plan. Des.* **2006**, *33*, 705–725. [CrossRef]
68. Boeing, G. OSMnx: New methods for acquiring, constructing, analyzing, and visualizing complex street networks. *Comput. Environ. Urban Syst.* **2017**, *65*, 126–139. [CrossRef]
69. Zhao, P.; Yen, Y.; Bailey, E.; Sohail, M. Analysis of urban drivable and walkable street networks of the ASEAN Smart Cities Network. *ISPRS Int. J. Geo-Inf.* **2019**, *8*, 459. [CrossRef]
70. Aitchison, J. The statistical analysis of compositional data. *J. R. Stat. Soc. Ser. B (Methodol.)* **1982**, *44*, 139–160. [CrossRef]
71. Zhou, H.; Chen, Y.; Tian, R. Land-use conflict identification from the perspective of construction space expansion: An evaluation method based on "Likelihood-Exposure-Consequence". *ISPRS Int. J. Geo-Inf.* **2021**, *10*, 433. [CrossRef]
72. Hou, L.; Xia, F.; Chen, Q.; Huang, J.; He, Y.; Rose, N.; Rozelle, S. Grassland ecological compensation policy in China improves grassland quality and increases herders' income. *Nat. Commun.* **2021**, *12*, 4683. [CrossRef] [PubMed]
73. He, Z.; Zhao, C.; Fürst, C.; Hersperger, A.M. Closer to causality: How effective is spatial planning in governing built-up land expansion in Fujian Province, China? *Land Use Policy* **2021**, *108*, 105562. [CrossRef]
74. Chen, L.; Cai, H. Study on land use conflict identification and territorial spatial zoning control in Rao River Basin, Jiangxi Province, China. *Ecol. Indic.* **2022**, *145*, 109594. [CrossRef]
75. Olumba, C.N.; Rickson, J.R.; Rabinovich, A.; Lind, J.; Mtei, K.; Nebiyu, A.; Leal, A.; Drury, J.; Borgerhoff Mulder, M.; Meya, A.; et al. Comparing participatory and expert-led decisions: Insights from participatory planning of nature-based solutions for advancing land degradation neutrality in northern Tanzania. *Land Use Policy* **2026**, *171*, 108234. [CrossRef]
76. Malczewski, J.; Jankowski, P. Emerging trends and research frontiers in spatial multicriteria analysis. *Int. J. Geogr. Inf. Sci.* **2020**, *34*, 1257–1282. [CrossRef]
77. Lei, Y.; Flacke, J.; Schwarz, N. Does urban planning affect urban growth pattern? A case study of Shenzhen, China. *Land Use Policy* **2021**, *101*, 105100. [CrossRef]
78. Sun, P.; Mo, J.; Li, N.; Hou, D.; Liu, Q. Spatial–temporal evolution and driving mechanism of territorial space conflicts in rapid urbanization areas from the perspective of suitability: An empirical study of Jinan City, China. *Land* **2026**, *15*, 191. [CrossRef]

Disclaimer/Publisher's Note: The statements, opinions and data contained in all publications are solely those of the individual author(s) and contributor(s) and not of MDPI and/or the editor(s). MDPI and/or the editor(s) disclaim responsibility for any injury to people or property resulting from any ideas, methods, instructions or products referred to in the content.